



## Research paper

## Hit-to-lead optimization of a latency-associated nuclear antigen inhibitor against Kaposi's sarcoma-associated herpesvirus infections

Philine Kirsch<sup>a, b, c</sup>, Saskia C. Stein<sup>c, d</sup>, Aylin Berwanger<sup>a, b, c</sup>, Julia Rinkes<sup>a, b, c</sup>,  
Valentin Jakob<sup>a, b, c</sup>, Thomas F. Schulz<sup>c, d</sup>, Martin Empting<sup>a, b, c, \*</sup>

<sup>a</sup> Department of Drug Design and Optimization (DDOP), Helmholtz-Institute for Pharmaceutical Research Saarland (HIPS) - Helmholtz Centre for Infection Research (HZI), Campus E8.1, 66123, Saarbrücken, Germany

<sup>b</sup> Department of Pharmacy, Saarland University, Campus E8.1, 66123, Saarbrücken, Germany

<sup>c</sup> German Centre for Infection Research (DZIF), Partner Site Hannover-Braunschweig, 66123, Saarbrücken, Germany

<sup>d</sup> Institute of Virology, Hannover Medical School, Carl-Neuberg-Strasse 1, 30625, Hannover, Germany

## ARTICLE INFO

## Article history:

Received 11 February 2020

Received in revised form

25 May 2020

Accepted 30 May 2020

Available online 28 June 2020

## Keywords:

Hit-to-lead optimization

Latency-associated nuclear antigen (LANA)

Kaposi's sarcoma herpesvirus (KSHV)

Fluorescence polarization (FP)-Based

interaction inhibition assay

Electrophoretic mobility shift assay (EMSA)

CuAAC

STD-NMR

## ABSTRACT

The Latency-associated nuclear antigen (LANA) plays a central role for the latent persistence of the Kaposi's Sarcoma Herpesvirus (KSHV) in the human host and helps to establish lifelong infections. Herein, we report our efforts towards hit-to-lead generation starting from a previously discovered LANA-DNA inhibitor. By tethering the viral genome to the host nucleosomes, LANA ensures the segregation and persistence of the viral DNA during mitosis. LANA is also required for the replication of the latent viral episome during the S phase of the cell cycle. We aim to inhibit the interaction between LANA and the viral genome to prevent the latent persistence of KSHV in the host organism. Medicinal chemistry-driven optimization studies and structure-activity-relationship investigation led to the discovery of an improved LANA inhibitor. The functional activity of our compounds was evaluated using a fluorescence polarization (FP)-based interaction inhibition assay and electrophoretic mobility shift assay (EMSA). Even though a crystal structure of the ligand protein complex was not available, we successfully conducted hit optimization toward a low micromolar protein-nucleic acid-interaction inhibitor. Additionally, we applied STD-NMR studies to corroborate target binding and to gain insights into the binding orientation of our most potent inhibitor, providing opportunities for further rational design of more efficient LANA-targeting anti KSHV agents in future studies.

© 2020 The Author(s). Published by Elsevier Masson SAS. This is an open access article under the CC BY-NC-ND license (<http://creativecommons.org/licenses/by-nc-nd/4.0/>).

## 1. Introduction

Kaposi's Sarcoma Herpesvirus (KSHV) is a human gamma herpesvirus and establishes a lifelong latent infection in B-cells and endothelial cells [1,2]. The virus was identified as the etiological agent of Kaposi's Sarcoma (KS) and is involved in two other neoplastic diseases, multicentric Castleman's disease and pleural effusion lymphoma [1,3]. In healthy individuals, KSHV-associated diseases are rare. However, in immunosuppressed patients, e.g., transplant recipients or patients with the acquired immunodeficiency syndrome (AIDS), KSHV is highly oncogenic [4,5]. However,

classic KS mainly can also occur in elderly men especially from KSHV-endemic areas and endemic KS in East and Central Africa [6]. The main key player for the establishment and maintenance of the latent infection is the latency-associated nuclear antigen (LANA) [7–9]. It is an origin-binding protein, whose C-terminal domain binds to the viral genome and whose N-terminal region interacts simultaneously with host nucleosomes [10–12]. This allows the segregation of latent viral episomes during mitosis and their partitioning to daughter cells [13]. LANA has also additional functions like latent viral replication, transcriptional control and survival in the host cell [14–16]. The C-terminal DNA-binding domain (DBD) of LANA binds the viral genome in a sequence-specific manner [17]. Located on the terminal repeats (TRs) are three specific LANA binding sites (LBS), LBS1, LBS2 and LBS3. LBS1 has a hundred fold higher affinity to LANA compared to LBS2 and LBS3 [17]. In the majority of KSHV-associated cancer cells the viral genome is present and LANA is expressed [18]. It has been shown, that the

\* Corresponding author. Department of Drug Design and Optimization (DDOP), Helmholtz-Institute for Pharmaceutical Research Saarland (HIPS) - Helmholtz Centre for Infection Research (HZI), Campus E8.1, 66123, Saarbrücken, Germany.

E-mail address: [Martin.Empting@helmholtz-hzi.de](mailto:Martin.Empting@helmholtz-hzi.de) (M. Empting).

Abbreviations			
AIDS	acquired immune deficiency syndrome	KS	Kaposi Sarcoma
CTD	C-terminal domain	KSHV	Kaposi's sarcoma-associated herpesvirus
DCM	dichloromethane	LANA	latency-associated nuclear antigen
DMSO	dimethylsulfoxide	LBS	LANA binding site
DBD	DNA binding domain	LCMS	liquid chromatography mass spectrometer
DMF	dimethylformamide	MeCN	acetonitrile
DIPEA	diisopropylethylamine	MeOH	methanol
EE	ethyl acetate	MST	microscale thermophoresis
EtOH	ethanol	PBS	phosphate-buffered saline
EMSA	electrophoretic mobility shift assay	PE	petroleum benzene
FA	formic acid	STD NMR	saturation transfer difference nuclear magnetic resonance
FP	fluorescence polarization	SPR	surface plasmon resonance
HPLC	high pressure liquid chromatography	TR	terminal repeat
HHV-8	human herpesvirus 8	wt	wild-type

persistence of viral DNA is affected by disturbing or influencing LANA [15]. The inhibition of the interaction between LANA and viral DNA could lead to a reduction or loss of viral genomes in the infected cells. Today's treatment of KSHV and KSHV-associated diseases is difficult and still limited [19,20]. It is clear, that there is an urgent need for specific drugs, which interfere with novel steps in the KSHV lifecycle. In view of its central role during latent viral persistence, LANA is considered to be a very promising target for the development of specific antiviral therapeutics against KSHV.

In a study previously published by us in 2019, we described the discovery of first inhibitors, which interfere with the LANA-DNA interaction [11]. Further inhibitor scaffolds have been identified using a functional screen and an in-house compound library [21]. Starting with a fragment-based drug discovery approach, we successfully developed a fragment-sized inhibitor **I** capable to compete with the viral DNA (Fig. 1). For the evaluation of functional activity of our compounds, we used a fluorescence-polarization (FP)-based assay and electrophoretic mobility shift assay (EMSA) experiments. For our most promising fragment-sized inhibitor **I**, we observed an  $IC_{50}$  value of  $17 \pm 1 \mu\text{M}$  in our FP-assay using a LANA DNA binding domain (DBD) mutant and  $435 \pm 6 \mu\text{M}$  in the EMSA studies using the wild-type LANA C-terminal domain (CTD).

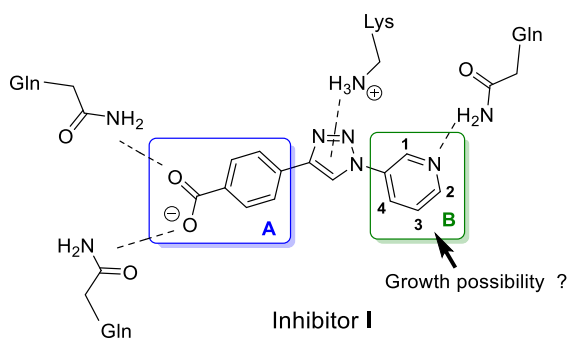
We confirmed target binding using microscale thermophoresis (MST) and saturation transfer difference (STD)-NMR experiments. Additionally, the STD-NMR experiments and molecular docking

studies provided important information on the putative orientation of Inhibitor **I** when bound to LANA. Based on the STD-NMR studies and docking results we suggested that the nitrogen at the pyridine core acts as a hydrogen bond acceptor and protons 2, 3 and 4 are not in direct interaction with the protein surface, hence these positions should be further investigated as potential growth vectors. Furthermore, two glutamines are presumably involved in hydrogen-bond interactions with the carboxyl group. However, it was not clear whether the carboxylic acid function is necessary for binding [11].

Based on these findings, we embarked on structure-activity relationship (SAR) studies and further medicinal chemistry optimization to improve the potency of our hit compounds. Herein, we report our recent advances in improving our LANA-DNA-interaction inhibitors using compound **I** as a starting point. Unfortunately, our efforts in solving a co-crystal structure of inhibitor **I** in complex with LANA have not been successful to date. This renders unambiguous experiment-supported structure-based optimization unfeasible. Therefore, we systematically investigated the LANA-DNA-interaction inhibition of new synthesized compounds using FP-based competition assay and EMSA experiments as the SAR drivers.

## 2. Design concept

Based on the previously applied STD-NMR and docking studies we modified Inhibitor **I** in a step-by-step manner. Inhibitor **I** was divided in two regions, the benzoic acid part **A** and the pyridine core **B** (Fig. 1). The triazole core was not yet modified in order to exploit the robust and facile Copper(I)-catalyzed azide-alkyne cycloaddition (CuAAC) click chemistry. First, region **A** was modified and variations of the carboxylic acid were introduced. As a second step, we have modified the pyridine moiety, region **B**. From our previous results we assumed that the nitrogen at the pyridine motif is essential for binding and functions as hydrogen bond acceptor. STD-NMR data revealed that Proton 1 interacts tightly with LANA while proton 2 is also in close proximity to the protein surface. However, our docking studies suggested that the latter might be at least partially solvent exposed. In contrast, protons at position 3 and 4 did not show direct contact with the LANA surface according to their weak STD-NMR effects. These observations inspired us to investigate positions 2, 3 and 4 as potential growth vectors in the presented study.



**Fig. 1.** Previously described LANA-DNA interaction inhibitor **I** and its predicted binding mode which provides the basis for structural optimization by rational design and growth vector exploration.

### 3. Results and discussion

#### 3.1. Chemistry

##### 3.1.1. Modifications of region A

3-azidopyridine **2** was generated by a standard azidation method using 3-aminopyridine **1**, NaNO<sub>2</sub> and NaN<sub>3</sub> in a mixture of EtOAc and 6M HCl [11,22]. In a second step, as depicted in Scheme 1, various commercially available ethynylbenzene derivatives were used in a standard copper-catalyzed CuAAC reaction with 3-azidopyridine to provide the triazoles **3–5**, **8**, **10**, **11**, and **13** [11].

The ethyl ester **6** and amide **7** analogue were generated from the carboxylic acid **3** by thionyl chloride-mediated activation and subsequent treatment with ethanol or aq. ammonia solution. The hydrolysis of 3-chloro-4-methylester intermediate **8** with NaOH in ethanol produced the corresponding acid **9**. The *N*-acetyl analogue **12** was synthesized from amine **11** with acetyl chloride under basic conditions.

##### 3.1.2. Modifications of region B

Compound **16** bearing an additional CH<sub>2</sub>-linker between triazole and pyridine core was synthesized starting from (bromo-methyl)benzene **14**, which was converted to the azide **15** using NaN<sub>3</sub> in DMSO [23], followed by a click reaction with 4-ethynylbenzoic acid. Different arylazides **17a-n** and **20** decorated with various substitutions were generated by reaction of the corresponding commercially available amines **18a-n** and **21** with NaNO<sub>2</sub> and NaN<sub>3</sub> in 6 M HCl and EtOAc (Scheme 2). The subsequent CuAAC click reaction with 4-ethynylbenzoic acid provided the target molecules **19a-n** and **22**. The hydroxypyridine **19o** analogue was generated from the methoxypyridine **19k** by treating with 48% aqueous HBr solution at 80 °C.

As depicted in Scheme 3, the syntheses of target compounds via Suzuki coupling was achieved using two different synthetic routes. In route 1, Suzuki coupling with different commercially available boronic acids and halogenated pyridine-3-amines **23**, **27** and **28** in presence of Pd(PPh<sub>3</sub>)<sub>4</sub> achieved phenyl-substituted pyridine amines **24a-b** and **29a-b** in the first step. Subsequently, the amines were converted to the corresponding azides **25a-b** and **30a-b** followed by a CuAAC click reaction with 4-ethynylbenzoic acid to obtain the target compounds **26a-b** and **31a-b**. In parallel, the alternative route 2 was established for late stage modifications via Suzuki coupling. First, halogenated pyridine-3-amines **32a-b** were converted to the corresponding azide **33a-b**, followed by click reaction with 4-ethynylbenzoate to obtain the corresponding triazole intermediates **34a-b**. Subsequently, phenyl-substituted compounds **35a-k** were achieved via Suzuki coupling using corresponding boronic acids and Pd(PPh<sub>3</sub>)<sub>4</sub>.

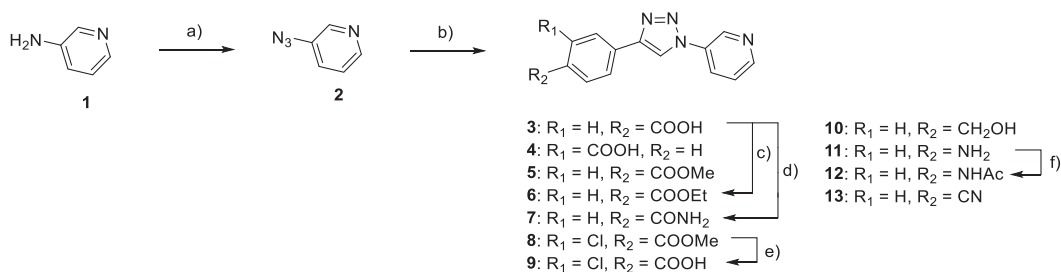
Finally, the hydrolysis of the esters with NaOH in methanol produced the target carboxylic acid compounds **36a-k**. As depicted in Scheme 4, for the synthesis of the series of pyridine-phenoxy target compounds **40a-e**, copper-catalyzed Ullmann reaction was used in the first step using 6-bromo-4-methylpyridin-3-amine **37**, the corresponding phenol derivative or thiophenol, Cs<sub>2</sub>CO<sub>3</sub> and CuI to obtain the aminopyridine-phenoxy intermediates **38a-e**.

The obtained amines were transformed into the corresponding azides **39a-e** as described above. Last step was a CuAAC reaction of azides with 4-ethynylbenzoic acid to obtain the target compounds **40a-e**. The isoquinoline **43** and quinoline **46** analogue were synthesized starting from isoquinoline-4-amin **41** and quinoline-3-amin **44** by standard azidation to **42** and **45**, followed by CuAAC click reaction with 4-ethynylbenzoic acid. Further isoquinoline derivatives **50a-c** were synthesized in a 3 step procedure (Scheme 5). A direct transformation of bromo isoquinolines **47a-c** into the corresponding azides using NaN<sub>3</sub>, Cu(I) and Na<sub>2</sub>CO<sub>3</sub> at 85 °C over night as described in literature was not efficient [24]. LCMS-guided reaction monitoring showed the formation the primary amine and other side products. For this reason, we extended the reaction time until we detected full conversion into the corresponding primary amine **48a-c** with the aim to subsequently transform these intermediates into the corresponding azides. Indeed, we achieved successful azidation (intermediates **49a-c**) and CuAAC coupling, respectively, using amines **48a-c** and the conditions described above yielding the desired isoquinoline products **50a-c**.

#### 3.2. Functional evaluation using LANA-DNA interaction inhibition assays and SAR studies

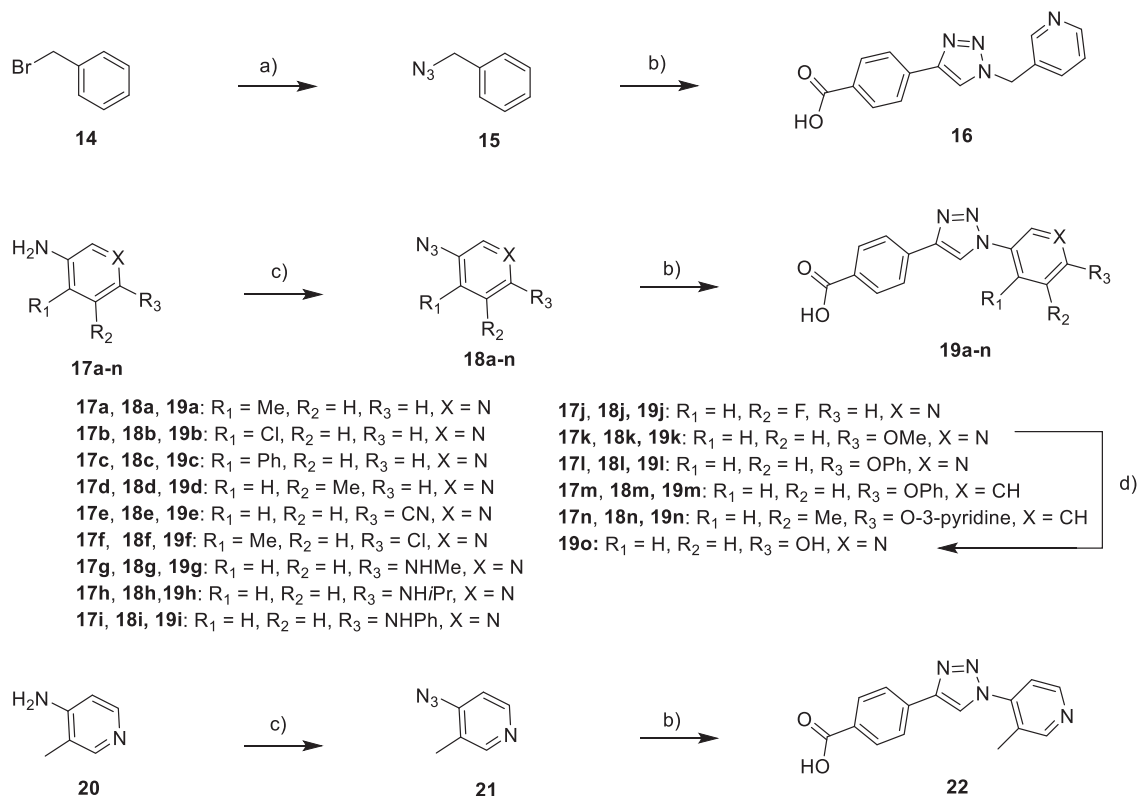
The target compounds were tested for functional activity in the FP-based LANA-DNA interaction inhibition assay using LBS2 as the probe and an oligomerization-deficient LANA DBD mutant [11]. This oligomerization-deficient C-terminal LANA mutant (aa1008-1146) has nine amino acid point mutations: K1055E, K1138S, K1140D, K1141D, R1039Q, R1040Q, A1121E, K1109A, and D1110A. For this mutant, also in presence of oligonucleotides, which represent the viral LANA-binding sites LBS1, LBS2 or LBS3, a high water solubility was shown [10,11,17,25]. All compounds showing an IC<sub>50</sub> values less than 250 μM were further tested in an orthogonal LANA-DNA interaction inhibition assay employing EMSA methodology, the same LANA DBD mutant and LBS1 as probe. As described above, the latter oligo has a higher affinity to the target rendering the EMSA experiment a more stringent read out for compound efficacy.

For the first series of compounds, we investigated the significance of the carboxylic acid in the Western part of the molecule (region A) by varying its position, attaching additional groups or substituting it by other polar functional groups capable of



**Scheme 1.** Modification of region A.<sup>a</sup>

<sup>a</sup>Reagents and conditions: a) NaNO<sub>2</sub>, NaN<sub>3</sub>, EtOAc, 6M HCl, 0 °C → rt, yield 50%; 2 h; b) corresponding ethynylbenzene, CuSO<sub>4</sub>•5H<sub>2</sub>O, Na-Ascorbate, DIPEA, MeOH, H<sub>2</sub>O, rt, 16 h, yield 60–82%; c) 1. SOCl<sub>2</sub>, DMF, 60 °C, 1 h, 2. EtOH, DIPEA, rt, 16 h, yield 53%; d) 1. SOCl<sub>2</sub>, DMF, 60 °C, 1 h, 2. NH<sub>4</sub>OH, rt, 16 h, yield 27%; e) 2 M NaOH, MeOH, rt, 16 h, yield 66%; f) Acetyl chloride, Et<sub>3</sub>N, DCM, DMF, rt, 16 h, yield 14%.



**Scheme 2.** Azide synthesis and CuAAC click reaction.<sup>a</sup>

<sup>a</sup>Reagents and conditions: a) NaN<sub>3</sub>, Et<sub>3</sub>N, DMSO, rt, 16 h, yield 78%; b) 4-ethynylbenzoic acid, CuSO<sub>4</sub>•5H<sub>2</sub>O, Na-Ascorbate, DIPEA, MeOH, H<sub>2</sub>O, rt, 16 h, yield 20–90%; c) NaNO<sub>2</sub>, NaN<sub>3</sub>, EtOAc, 6M HCl, 0 °C → rt, 2 h, yield 4–98%; d) 48% aq. HBr, 80 °C, 12 h, yield 86%.

participating in hydrogen bonding. The results are shown in Table 1.

Moving the carboxylic acid from *para* (inhibitor **1**) to *meta* position (**4**) decreases the activity significantly. Also an additional chlorine atom attached in *meta* position (**9**) lead to a complete loss of activity. The replacement of the carboxylic acid by a methyl ester (**5**), ethyl ester (**6**) or amide (**7**) was also detrimental. Furthermore, moving from the carboxylic acid to the methyl alcohol (**10**), amine (**11**), acetamide (**12**) or nitrile (**13**) also resulted in inactive compounds. These results indicate that the carboxylic acid in *para* position in region A is essential for inhibitory activity. Therefore, we kept the *p*-carboxylic acid in region A fixed for further optimization studies and focused on the modifications at the pyridine core in region B. First, we examined the effect on inserting a short linker between the triazole and the pyridine core (**16**).

This, however, resulted in loss of activity. As described before, from previous STD-NMR and molecular docking experiments we expected, that growing the fragment-sized Inhibitor **1** in different positions at the pyridine core (region B) would potentially increase potency.

To explore the influence of larger structural motifs at the pyridine core in position 4 we introduced a variety of residues. As listed in Table 2, growing in this position is accepted and resulted in moderate to potent inhibitory effects in FP assay ranging from IC<sub>50</sub> values of 86 ± 6 μM (**19a**) to 18 ± 4 μM (**19c**). The size of the introduced residue seems to play an important role. While a small methyl group is not favorable, but accepted (**19a**, IC<sub>50</sub> 86 ± 6 μM), further increasing the size from chlorine (**19b**) to phenyl (**19c**) improves IC<sub>50</sub> values to 29 ± 1 μM and 18 ± 4 μM, respectively. This observation might hint at a steric *ortho* effect. The additional bulky phenyl ring strongly hinders the rotation of the bond between triazole and pyridine and, therefore, might fix the nitrogen

in the pyridine core in a more favorable orientation. In EMSA experiments, 4-substituted compounds **19b** (EMSA: 94% inhibition @ 500 μM) and **19c** (EMSA: 100% inhibition @ 500 μM) showed a higher efficiency compared to Inhibitor **1** (EMSA: 83% inhibition @ 500 μM) [11]. Additionally, we shifted the nitrogen of the pyridine core from *meta* (**19a**) to *para* position (**22**) which resulted in an inactive compound. The improvements in the EMSA assay for compounds **19b-c** over our initial hit compound **1** were not perfectly mirrored by the FP IC<sub>50</sub> values, which presumably is rooted in the usage of different DNA probes (LBS1 vs LBS2, respectively).

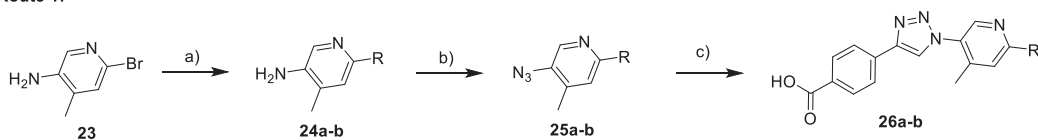
Nevertheless, the results for compounds **19b** and **19c** were a major step towards achieving LANA inhibitors suitable for cellular assays and encouraged us to explore the potential of growing the hit scaffold in this direction even further.

In the next series of compounds, Inhibitor **1** was grown in position 3 at the pyridine core by introducing a variety of aromatic rings. As listed in Table 3, a small methyl residue in position 3 (**19d**, IC<sub>50</sub> of 45 ± 5 μM; EMSA: 78% inhibition @ 500 μM) is tolerated, but the fluorinated analogue **19j** and most of the phenyl substituted compounds **36a-d**, **36f-i**, and **31a** showed a complete loss or only moderate activity.

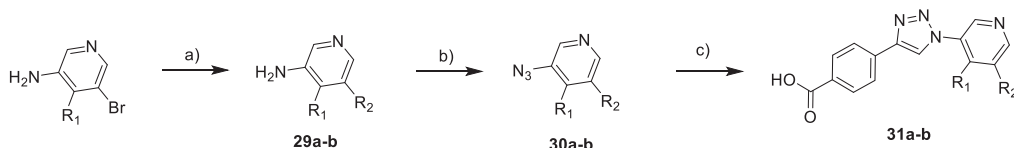
However, compounds with an additional hydroxyl function attached to the phenyl ring (**36e**, IC<sub>50</sub> of 153 ± 7 μM, EMSA: 20% inhibition @ 500 μM) showed moderate activity.

Moving from a phenyl **36a** to a smaller and more polar furanyl residue **36j** the potency was restored (IC<sub>50</sub> of 19 ± 2 μM). Unfortunately, in EMSA experiments we observed only a weak effect (34% inhibition @ 500 μM) for this compound. Interestingly, by attaching an additional chlorine atom in position 4 and having a phenyl in position 3 (**31b**) resulted in a highly potent compound with IC<sub>50</sub> of

## Route 1:



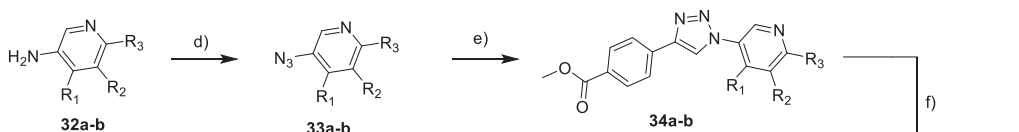
24a, 25a, 26a: R = 2-phenol  
24b, 25b, 26b: R = 3-(hydroxymethyl)phenyl



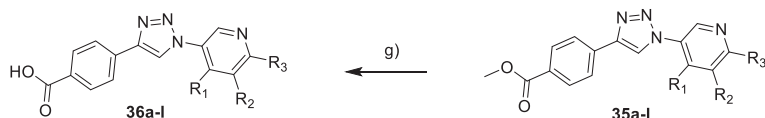
27: R<sub>1</sub> = H, R<sub>2</sub> = Br, R<sub>3</sub> = H  
28: R<sub>1</sub> = Cl, R<sub>2</sub> = Br, R<sub>3</sub> = H

29a, 30a, 31a: R<sub>1</sub> = H, R<sub>2</sub> = 3-(hydroxymethyl)phenyl  
29b, 30b, 31b: R<sub>1</sub> = Cl, R<sub>2</sub> = Ph

## Route 2:



32a, 33a, 34a: R<sub>1</sub> = H, R<sub>2</sub> = Br, R<sub>3</sub> = H  
32b, 33b, 34b: R<sub>1</sub> = Me, R<sub>2</sub> = H, R<sub>3</sub> = Cl

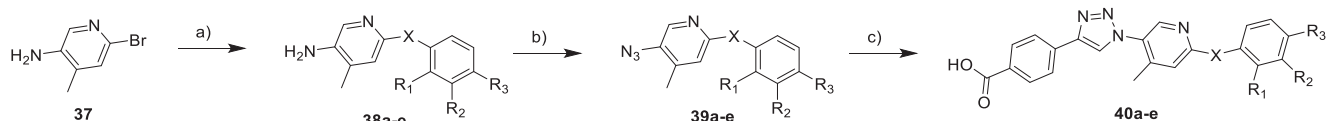


35a, 36a: R<sub>1</sub> = H, R<sub>2</sub> = Ph, R<sub>3</sub> = H  
35b, 36b: R<sub>1</sub> = H, R<sub>2</sub> = 2-methoxyphenyl, R<sub>3</sub> = H  
35c, 36c: R<sub>1</sub> = H, R<sub>2</sub> = 3-methoxyphenyl, R<sub>3</sub> = H  
35d, 36d: R<sub>1</sub> = H, R<sub>2</sub> = 4-methoxyphenyl, R<sub>3</sub> = H  
35e, 36e: R<sub>1</sub> = H, R<sub>2</sub> = 3-hydroxyphenyl, R<sub>3</sub> = H  
35f, 36f: R<sub>1</sub> = H, R<sub>2</sub> = 3,4-dimethylphenyl, R<sub>3</sub> = H

35g, 36g: R<sub>1</sub> = H, R<sub>2</sub> = 3,4-difluorophenyl, R<sub>3</sub> = H  
35h, 36h: R<sub>1</sub> = H, R<sub>2</sub> = 4-(hydroxymethyl)phenyl, R<sub>3</sub> = H  
35i, 36i: R<sub>1</sub> = H, R<sub>2</sub> = 3-fluoro-5-methoxyphenyl, R<sub>3</sub> = H  
35j, 36j: R<sub>1</sub> = H, R<sub>2</sub> = 3-furanyl, R<sub>3</sub> = H  
35k, 36k: R<sub>1</sub> = Me, R<sub>2</sub> = H, R<sub>3</sub> = Ph  
35l, 36l: R<sub>1</sub> = Me, R<sub>2</sub> = H, R<sub>3</sub> = 4-chlorobenzene

**Scheme 3.** Synthesis of target compounds via Suzuki coupling using two different routes.<sup>a</sup>

<sup>a</sup>Reagents and conditions: a) corresponding boronic acid, Na<sub>2</sub>CO<sub>3</sub>, Pd(PPh<sub>3</sub>)<sub>4</sub>, 1,4-dioxan, H<sub>2</sub>O, 90 °C, 16 h, yield 21–75%; b) NaNO<sub>2</sub>, NaN<sub>3</sub>, EtOAc, 6M HCl, 0 °C → rt, 2 h, yield 86–99%; c) 4-ethynyl benzoic acid, CuSO<sub>4</sub>•5H<sub>2</sub>O, Na-Ascorbate, DIPEA, MeOH, H<sub>2</sub>O, rt, 16 h, yield 63–80%; d) NaNO<sub>2</sub>, NaN<sub>3</sub>, EtOAc, 6M HCl, 0 °C → rt, 2 h, yield 34–80%; e) 4-ethynyl benzoate, CuSO<sub>4</sub>•5H<sub>2</sub>O, Na-Ascorbate, DIPEA, MeOH, H<sub>2</sub>O, rt, 16 h, yield 63–80%; f) corresponding boronic acid, Na<sub>2</sub>CO<sub>3</sub>, Pd(PPh<sub>3</sub>)<sub>4</sub>, 1,4-dioxan, H<sub>2</sub>O, 90 °C, 16 h, yield 20–90%; g) 2 M NaOH, MeOH, rt, 16 h, yield 16–83%.



38a, 39a, 40a: R<sub>1</sub> = H, R<sub>2</sub> = H, R<sub>3</sub> = H, X = O  
38b, 39b, 40b: R<sub>1</sub> = F, R<sub>2</sub> = H, R<sub>3</sub> = H, X = O  
38c, 39c, 40c: R<sub>1</sub> = H, R<sub>2</sub> = F, R<sub>3</sub> = H, X = O  
38d, 39d, 40d: R<sub>1</sub> = H, R<sub>2</sub> = H, R<sub>3</sub> = F, X = O  
38e, 39e, 40e: R<sub>1</sub> = H, R<sub>2</sub> = H, R<sub>3</sub> = H, X = S

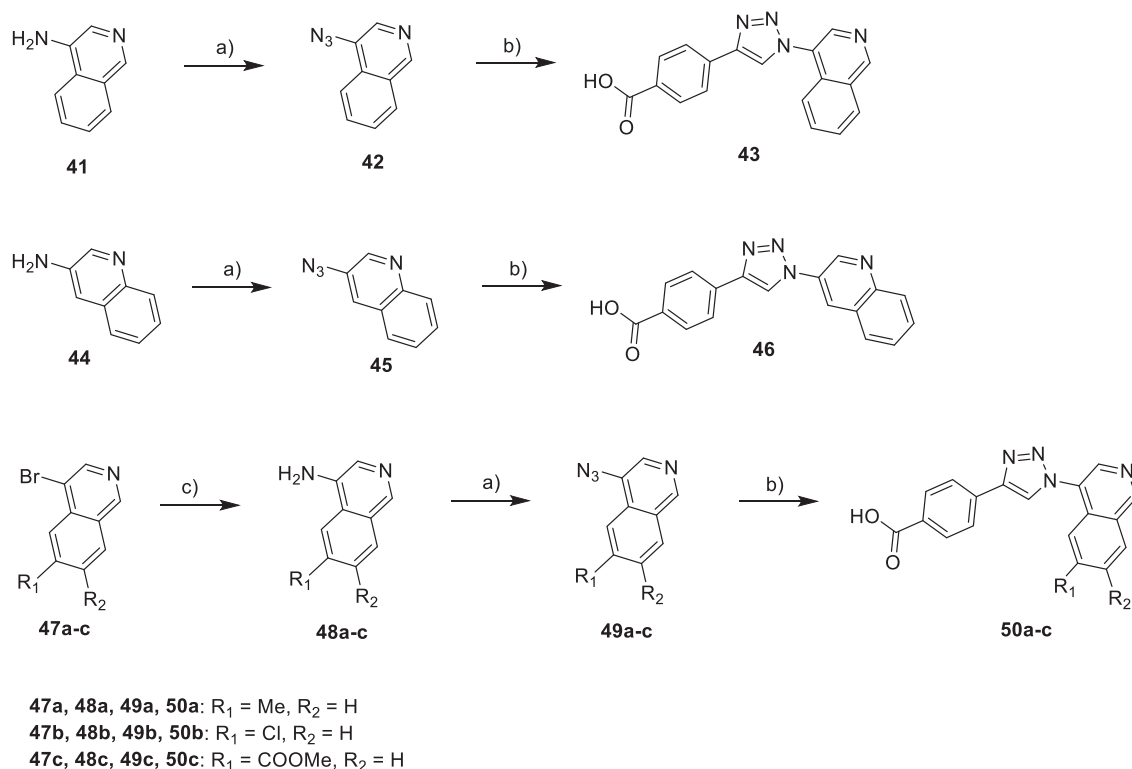
**Scheme 4.** Synthesis of target compounds via Ullmann Reaction.<sup>a</sup>

<sup>a</sup>Reagents and conditions: a) corresponding phenol or thiophenol, Cs<sub>2</sub>CO<sub>3</sub>, CuI, DMF, 130 °C, 16 h, yield 28–94%; b) NaNO<sub>2</sub>, NaN<sub>3</sub>, EtOAc, 6M HCl, 0 °C → rt, 2 h, yield 70–99%; c) 4-ethynyl benzoic acid, CuSO<sub>4</sub>•5H<sub>2</sub>O, Na-Ascorbate, DIPEA, MeOH, H<sub>2</sub>O, rt, 16 h, yield 45–93%.

38 ± 3 μM and full inhibition in FP and EMSA assays, respectively. These results further corroborate the notion of a beneficial *ortho* effect.

To explore the influence of growing inhibitor **I** at the pyridine core in position 2, a set of different target compounds was synthesized (Tables 3 and 4). The direct attachment of a nitrile group to the pyridine was tolerated (**19e**: IC<sub>50</sub> 52 ± 37 μM, EMSA: n. i.).

Moving to chlorine, hydroxy or methoxy group we observed a significant loss in activity (**19f**: IC<sub>50</sub> > 250 μM; **19o**: IC<sub>50</sub> 214 ± 24 μM and **19k**: IC<sub>50</sub> 218 ± 192 μM). Also in EMSA experiments **19j** (75% inhibition @ 500 μM) and **19k** (11% inhibition @ 500 μM) did not show a significant effect. An increase in activity was observed by introducing bulkier substituents and an additional methyl group for R<sub>1</sub>. In detail, an unpolar bulky phenyl or *p*-



**Scheme 5.** Synthesis of isoquinoline derivatives.<sup>a</sup>

<sup>a</sup>Reagents and conditions: a) NaNO<sub>2</sub>, NaN<sub>3</sub>, EtOAc, 6M HCl, 0 °C → rt, 2 h, yield 68–91%; b) 4-ethynyl benzoic acid, CuSO<sub>4</sub>•5H<sub>2</sub>O, Na-Ascorbate, DIPEA, MeOH, H<sub>2</sub>O, rt, 16 h, yield 25–90%; c) NaN<sub>3</sub>, Na<sub>2</sub>CO<sub>3</sub>, CuSO<sub>4</sub>•5H<sub>2</sub>O, Na-Ascorbate, L-proline, DMF, H<sub>2</sub>O, 85 °C, 24 h, yield 88–97%.

**Table 1**

Inhibition activities of compounds with modification in region A.

Cpd	R	FP Assay (LBS2) <sup>a</sup>		
		IC <sub>50</sub>	IC <sub>50</sub>	
<b>Inhibitor 1</b>		17 ± 1 μM	<b>9</b>	n.i.
<b>4</b>		>250 μM	<b>10</b>	n.i.
<b>5</b>		n.i. <sup>b</sup>	<b>11</b>	>250 μM
<b>6</b>		n.i.	<b>12</b>	n.i.
<b>7</b>		n.i.	<b>13</b>	>250 μM

<sup>a</sup> Fluorescence-polarization assay using LBS2 as probe, data representing average of duplicates ± standard deviation.

<sup>b</sup> No inhibition at 500 μM.

chlorophenyl was accepted in position 2 and we observed IC<sub>50</sub> values of 36 ± 5 μM for **36k** and 58 ± 7 μM for **36l** and moderate inhibition in EMSA. Analogues **26a** and **26b** with polar hydroxyl groups attached at the phenyl showed good potency with IC<sub>50</sub>

**Table 2**

Inhibitory activities of analogues modified in position 4 – observing higher efficiency for 4-substituted compounds.

Cpd	R	FP Assay (LBS2) <sup>a</sup>		EMSA (LBS1) <sup>b</sup> inhibition @ 500 μM
		IC <sub>50</sub>	IC <sub>50</sub>	
<b>Inhibitor 1</b>		17 ± 1 μM	82%	
<b>16</b>		>250 μM	n.d. <sup>d</sup>	
<b>19a</b>		86 ± 6 μM	39%	
<b>19b</b>		29 ± 1 μM	94%	
<b>19c</b>		18 ± 4 μM	100%	
<b>22</b>		n.i. <sup>c</sup>	n.d.	

<sup>a</sup> Fluorescence-polarization assay using LBS2 as probe, data representing average of duplicates ± standard deviation.

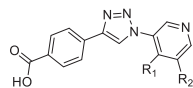
<sup>b</sup> Electrophoretic mobility shift assay using LBS1 as probe.

<sup>c</sup> No inhibition at 500 μM.

<sup>d</sup> Not determined.

**Table 3**

Inhibitory activities of analogues modified in position 3. Most derivatives substituted in this position (R<sub>2</sub>) showed a significant decrease in activity.



cpd	R <sub>1</sub>	R <sub>2</sub>	FP Assay (LBS2)	EMSA (LBS1)
			IC <sub>50</sub>	Inhibition @ 500 μM
<b>Inhibitor I</b>	H	H	17 ± 1 μM	82%
<b>19d</b>	H	Me	45 ± 5 μM	78%
<b>19j</b>	H	F	n. i.	n. d.
<b>36a</b>	H		>250 μM	n. d.
<b>36f</b>	H		n. i.	n. d.
<b>36g</b>	H		>250 μM	n. d.
<b>36b</b>	H		n. i.	n. d.
<b>36c</b>	H		110 ± 32 μM	n. i.
<b>36d</b>	H		n. i.	n. d.
<b>36i</b>	H		n. i.	n. d.
<b>36e</b>	H		153 ± 7 μM	20%
<b>31a</b>	H		>250 μM	n. d.
<b>36h</b>	H		>250 μM	n. d.
<b>36j</b>	H		19 ± 2 μM	34%
<b>31b</b>	Cl		38 ± 3 μM	100%

<sup>a</sup>Fluorescence-polarization assay using LBS2 as probe, data representing average of duplicates ± standard deviation.

<sup>b</sup>Electrophoretic mobility shift assay using LBS1 as probe.

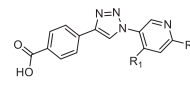
<sup>c</sup>No inhibition at 500 μM.

<sup>d</sup>Not determined.

values of 21 ± 3 μM and 25 ± 1 μM, respectively. Furthermore, the efficiency of these two analogues in our EMSA studies was high with a full inhibition @ 500 μM. By attaching methylamine (**19g**), isopropylamine (**19h**) and anilino (**19i**) at position 2 we observed an increase in activity from small to bigger size, whereby the methylamine compound **19g** was completely inactive and the

**Table 4**

Inhibitory activities of analogues modified in position 2. Attaching polar hydroxyl benzene groups increases inhibitory activity.



cpd	R <sub>1</sub>	R <sub>2</sub>	FP Assay (LBS2)	EMSA (LBS1)
			IC <sub>50</sub>	Inhibition @ 500 μM
<b>Inhibitor I</b>	H	H	17 ± 1 μM	82%
<b>19e</b>	H	CN	52 ± 37 μM	n. i.
<b>19f</b>	Me	Cl	>250 μM	n. d.
<b>19o</b>	H	OH	214 ± 24 μM	75%
<b>19k</b>	H	OMe	218 ± 192 μM	11%
<b>36k</b>	Me		36 ± 5 μM	36%
<b>36l</b>	Me		58 ± 7 μM	30%
<b>26a</b>	Me		21 ± 3 μM	100%
<b>26b</b>	Me		25 ± 1 μM	100%
<b>19g</b>	H		n. i.	n. d.
<b>19h</b>	H		>250 μM	n. d.
<b>19i</b>	H		110 ± 20 μM	29%

<sup>a</sup>Fluorescence-polarization assay using LBS2 as probe, data representing average of duplicates ± standard deviation.

<sup>b</sup>Electrophoretic mobility shift assay using LBS1 as probe.

<sup>c</sup>No inhibition at 500 μM.

<sup>d</sup>Not determined.

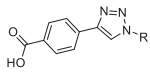
anilino analogue **19i** showed a moderate activity of IC<sub>50</sub> of 110 μM and 29% inhibition in EMSA.

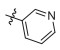
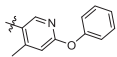
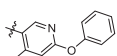

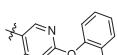
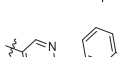
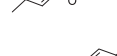
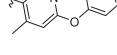
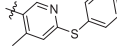
Additionally, a series of compounds was synthesized with a more flexible and bulky phenoxy group in position 2 (**Table 5**). The phenoxy analogue **19l**, similar to the aminophenyl compound **19i**, was inactive, indicating that an amino linker between pyridine and phenyl is more suitable for activity compared to the oxygen linker. By attaching an additional methyl group in position 4 (R<sub>1</sub>) at the pyridine core **40a** an increase in activity compared to **19l** was observed leading to a moderate IC<sub>50</sub> of 198 ± 8 μM. The fluorinated analogues **40b-d** also showed moderate activities like compound **40a** while the *o*-fluoro analogue **40b** possessed the best IC<sub>50</sub> of 64 ± 2 μM. For the *m*- (**40c**) and *p*-fluoro (**40d**) derivatives IC<sub>50</sub>s of 122 ± 3 μM and 134 ± 2 μM were observed, respectively. Unfortunately, all these compounds showed no effect in EMSA experiments.

Exchanging the oxygen linker by a sulfur (**40e**, IC<sub>50</sub> 175 ± 10 μM) was tolerated (compare with **40a**, IC<sub>50</sub> 198 ± 8 μM). As expected, by removing the nitrogen in the pyridine core resulted in an inactive compound (**19m**). Astonishingly, moving the nitrogen to the phenoxy residue (**19n**) yielded a highly potent compound with an IC<sub>50</sub> of 19 ± 1 μM showing also full inhibition in the EMSA experiments.

Intrigued by the notion that fragment growing in position 3 was possible in combination with *ortho*-substituents, we focused our efforts on further exploring these two positions by installing a connected structural motif. To this end, we designed and synthesized isoquinoline analogues (**Table 6**). In general, isoquinoline analogues were pleasingly effective. The unsubstituted isoquinoline

**Table 5**  
Inhibitory activities of Phenoxy analogues. Shifting nitrogen to the phenoxy residue improves inhibitory efficiency.



cpd	R <sub>2</sub>	FP Assay (LBS2)	EMSA (LBS1)
		IC <sub>50</sub>	inhibition @ 500 μM
<b>Inhibitor I</b>		17 ± 1 μM	82%
<b>19l</b>		n. i.	n. d.
<b>40a</b>		198 ± 8 μM	n. i.
<b>40b</b>		64 ± 2 μM	n. i.
<b>40c</b>		122 ± 3 μM	n. i.
<b>40d</b>		134 ± 2 μM	n. i.
<b>40e</b>		175 ± 10 μM	n. i.
<b>19m</b>		n.i.	n. d.
<b>19n</b>		19 ± 1 μM	100%

<sup>a</sup>Fluorescence-polarization assay using LBS2 as probe, data representing average of duplicates ± standard deviation.

<sup>b</sup>Electrophoretic mobility shift assay using LBS1 as probe.

<sup>c</sup>No inhibition at 500 μM.

<sup>d</sup>Not determined.

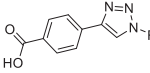
**43** showed an FP IC<sub>50</sub> value of 33 ± 1 μM and 96% inhibition in EMSA experiments. Moving from isoquinoline to quinoline **46** resulted in a slight loss in activity compared to **43** (**46**, IC<sub>50</sub> 70 ± 34 μM, 61% inhibition in EMSA).

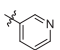
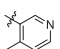
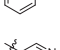
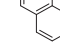
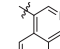
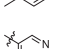
Attaching an additional methyl (**50a**) or chlorine (**50b**) at the isoquinoline motif was beneficial for the inhibitory effect. Noteworthy, **50a** showed the lowest FP IC<sub>50</sub> of 8 ± 1 μM reported to date, while **50b** also possessed a decent IC<sub>50</sub> of 17 ± 1 μM. Furthermore, in EMSA experiments 100% inhibition was detected for both compounds at 500 μM. Finally, an isoquinoline methylester analogue **50c** was inactive, however.

### 3.3. Further characterization and EMSA studies using wild-type LANA

For further evaluation and characterization the most promising compounds were selected. On the bases of our results, we chose compounds **19c**, **31b**, **26a-b**, **19n**, **50a**, and **50b**, which possessed the best IC<sub>50</sub> values in the FP-based assay and showed strong inhibitory effects at 500 μM in EMSA using the oligomerization-deficient LANA DBD mutant (aa1008-1146).

**Table 6**  
Inhibitory activities of Isoquinoline derivatives. Adding an annulated ring structure in direction of identified growth vector results in the most efficient inhibitors to date.



Cpd	R	FP Assay (LBS2)	EMSA (LBS1)
		IC <sub>50</sub>	inhibition @ 500 μM
<b>Inhibitor I</b>		17 ± 1 μM	82%
<b>43</b>		33 ± 1 μM	96%
<b>46</b>		70 ± 34 μM	61%
<b>50a</b>		8 ± 1 μM	100%
<b>50b</b>		17 ± 1 μM	100%
<b>50c</b>		>250 μM	n. d.

<sup>a</sup>Fluorescence-polarization assay using LBS2 as probe, data representing average of duplicates ± standard deviation; <sup>b</sup>Electrophoretic mobility shift assay using LBS1 as probe; <sup>c</sup>No inhibition at 500 μM; <sup>d</sup>Not determined.

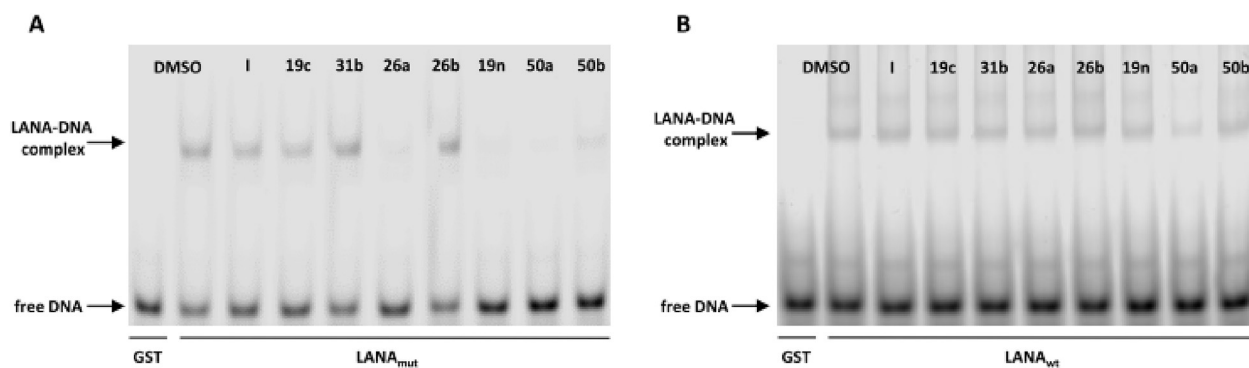
First, these compounds were initially tested for inhibition at 250 μM using LANA DBD mutant (Fig. 2, A) to see if they are also able to disturb the LANA-DNA interaction at a lower concentration in EMSA and compared these results also with inhibitor **I**. Inhibitor **I** and the compounds **19c**, **31b**, and **26b** showed no inhibitory effect on the LANA<sub>mut</sub>-DNA interaction at 250 μM. However, strong inhibitory effects were observed at this concentration for compounds **26a**, **19n**, **50a**, and **50b** as observed by the disappearance of the bands for the LANA<sub>mut</sub>-DNA complex (upper band, Fig. 2A).

We also determined the inhibitory activity of our best compounds against the interaction between wild-type LANA CTD (aa934-1162) and viral LBS1 (Fig. 2, B) in EMSA. Our wild-type LANA CTD construct is longer compared to the LANA DBD mutant and has no mutations and still shows a sufficient solubility in aqueous medium also in presence of viral LBS1. The compounds were also tested at 250 μM. Unfortunately, no inhibitory effect was observed for compounds **I**, **19c**, **31b**, **26a-b**, **19n**, and **50b**. However, Compound **50a** showed a significant effect and was able to inhibit the interaction between wild-type LANA CTD and LBS1.

Furthermore, we titrated the compounds showing an effective inhibition in EMSA using the LANA DBD mutant (Fig. 2, A), in EMSA experiments using the LANA DBD mutant and LBS1 as a probe to determine the IC<sub>50</sub> values. The results are listed in Table 7 and detailed information can be found in the supporting information.

As reported earlier by us, inhibitor **I** showed an IC<sub>50</sub> in FP assay (LBS2) of 17 ± 1 μM and an IC<sub>50</sub> in EMSA of 426 ± 2 μM using LANA DBD mutant [11]. The observed IC<sub>50</sub> values using LBS2 for the most promising inhibitors were basically in the same range. Additionally, we also tested the most promising inhibitors





**Fig. 2.** EMSA gels with inhibitor **I**, **19c**, **31b**, **26a-b**, **19n**, **50a-b**. Compounds were tested at a final concentration of 250  $\mu$ M and LBS1 was used as probe. (A) Using an oligomerization-deficient LANA DBD mutant, a strong inhibitory effect (disappearance of LANA-DNA complex band) was observed for compounds **26a**, **19n** and **50a-b** (B) Using wild-type LANA CTD, a significant inhibitory effect for compound **50a** was observed.

**Table 7**

Comparison of most efficient LANA-DNA inhibitors.

Cpd	Structure	FP-Assay <sup>a</sup> IC <sub>50</sub> (LBS2) (LANA <sub>mut</sub> )	FP-Assay IC <sub>50</sub> (LBS1) (LANA <sub>mut</sub> )	FP-Assay IC <sub>50</sub> (LBS3) (LANA <sub>mut</sub> )	EMSA <sup>b</sup> IC <sub>50</sub> (LBS1) (LANA <sub>mut</sub> )
<b>Inhibitor I</b>		17 ± 1 $\mu$ M	20 ± 3 $\mu$ M	19 ± 3 $\mu$ M	426 ± 2 $\mu$ M
<b>19c</b>		18 ± 4 $\mu$ M	52 ± 2 $\mu$ M	42 ± 3 $\mu$ M	n.i. at 250 $\mu$ M <sup>c</sup>
<b>31b</b>		38 ± 3 $\mu$ M	55 ± 7 $\mu$ M	45 ± 4 $\mu$ M	n.i. at 250 $\mu$ M
<b>26a</b>		21 ± 3 $\mu$ M	30 ± 2 $\mu$ M	34 ± 3 $\mu$ M	156 ± 27 $\mu$ M
<b>26b</b>		25 ± 1 $\mu$ M	64 ± 1 $\mu$ M	63 ± 8 $\mu$ M	n.i. at 250 $\mu$ M
<b>19n</b>		19 ± 1 $\mu$ M	15 ± 1 $\mu$ M	25 ± 1 $\mu$ M	64 ± 12 $\mu$ M
<b>50a</b>		8 ± 1 $\mu$ M	9 ± 2 $\mu$ M	8 ± 1 $\mu$ M	53 ± 43 $\mu$ M
<b>50b</b>		17 ± 1 $\mu$ M	14 ± 1 $\mu$ M	15 ± 1 $\mu$ M	93 ± 8 $\mu$ M

<sup>a</sup> Fluorescence-polarization assay using LBS1, LBS2 and LBS3 as probe, data representing average of duplicates ± standard deviation.

<sup>b</sup> Electrophoretic mobility shift assay using LBS1 as probe.

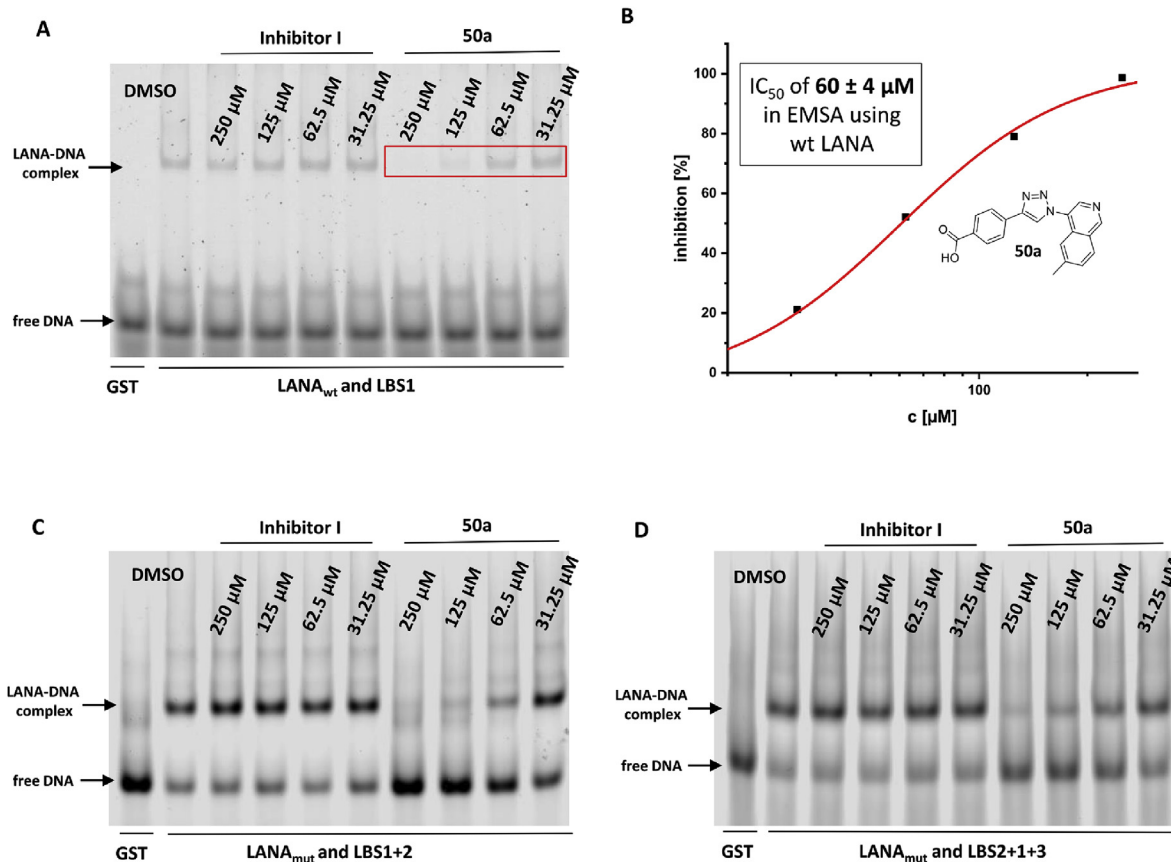
<sup>c</sup> No inhibition at 250  $\mu$ M.

in FP assay using LBS1 and LBS3, respectively. Compound **50a** showed a 2-fold better IC<sub>50</sub> of 8–9  $\mu$ M against all LBS compared to **I**. Furthermore, we could increase the inhibitory activity in EMSA experiments using LBS1 by 7-fold. As a consequence compounds **19n** and **50a** are the most potent LANA-LBS1-inhibitors reported so far (IC<sub>50</sub> values of 64 ± 12  $\mu$ M and 53 ± 3  $\mu$ M). Interestingly, compounds showing increased IC<sub>50</sub> values of 50–60  $\mu$ M against LBS1 and LBS3 in FP assay were also not effective in EMSA at 250  $\mu$ M. Excepted is however inhibitor **I**,

which showed also IC<sub>50</sub> values around 20  $\mu$ M against LBS1 and LBS3, but no effect at 250  $\mu$ M in EMSA.

As described above, only compound **50a** showed an inhibitory effect at a concentration of 250  $\mu$ M in EMSA using wild-type LANA CTD (Fig. 3 A). A dose-response EMSA experiment with wild-type LANA CTD yielded an IC<sub>50</sub> value of 60 ± 4  $\mu$ M (Fig. 3 B).

These results indicate that compound **50a** is equally potent against wild-type LANA CTD and the oligomerization-deficient LANA DBD mutant. In comparison to inhibitor **I** (IC<sub>50</sub> of



**Fig. 3.** (A) Dose-dependent EMSA experiment using wild-type LANA CTD, LBS1 as probe and Compound **50a**. (B) Curve shows normalized data points (inhibition from 0 to 100%) representing intensities of LANA-DNA-complex bands (Fig. 3 (A), upper bands, marked in red) from dose-dependent EMSA experiment.  $IC_{50}$  value was calculated using a four-parameter dose-response model. (C) Dose-dependent EMSA experiment using LANA DBD mutant, a combination of LBS1+2 as probe and Inhibitor **I** and Compound **50a**. (D) Dose-dependent EMSA experiment using LANA DBD mutant, a combination of LBS2+1 + 3 as probe and Inhibitor **I** and Compound **50a**. (For interpretation of the references to colour in this figure legend, the reader is referred to the Web version of this article.)

$435 \pm 6 \mu\text{M}$  against wild-type LANA CTD in EMSA) these results represent a huge potency improvement [11]. Furthermore, we tested if compound **50a** is also able to disturb the LANA-DNA interaction when using longer oligonucleotides comprising LBS1+2 as well as LBS2+1 + 3, in an arrangement that is present on the viral KSHV genome [17]. Each LBS is able to associate with one LANA dimer. Hence, LANA and the LBS1+2 oligomer can form a trimeric complex while the LBS2+1 + 3 oligomer gives rise to a quaternary complex. In order to test the efficacy of our inhibitors against the formation of these higher-order aggregates, dose-dependent EMSA experiments using LBS1+2 and LBS2+1 + 3 with the LANA DBD mutant were performed (Fig. 3C and D). We compared the effects of inhibitor **I** and Compound **50a** in this setup. As expected, inhibitor **I** showed no inhibitory effects in both experiments. However, Compound **50a** was still able to significantly inhibit the LANA LBS1+2 interaction at a concentration of  $62.5 \mu\text{M}$  (Fig. 3, C) and additionally inhibited the LANA LBS2+1 + 3 interaction at  $125 \mu\text{M}$  (Fig. 3, D). These results provide a basis for testing these inhibitors in cell based assays in the future.

The similar  $IC_{50}$  values of compound **50a** observed against wild-type LANA and LANA DBD mutant corroborates our hypothesis that our inhibitor binds at the DNA binding interface and is able to compete with the DNA. The DBD mutant involves nine point mutations, which are all located outside of the DNA binding site [25]. The goal of generating and using this mutant was to disturb the higher oligomerization in solution, which resulted in improved handling characteristics of the protein and better solubility of

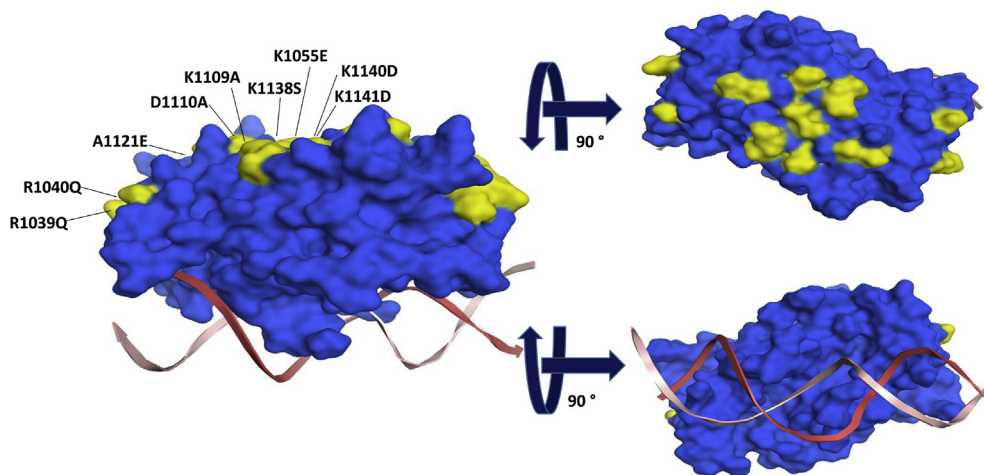
LANA-DNA complexes. Fig. 4 illustrates the LANA DBD surface (blue) and its single point mutations (yellow) bound to double-stranded DNA (red). The distribution of these mutations distant from the DNA-interaction interface combined with the observed similar  $IC_{50}$  values of our compound against wild-type and DBD mutant provide strong evidence, that we are targeting the LANA DNA interaction interface and that we do not unintentionally target one of the mutated regions on the LANA surface.

Taken together, compound **50a** is the most effective inhibitor against LANA DBD mutant and wild-type LANA CTD reported to date. To complement our studies, we applied STD-NMR experiments in order to identify further growth vectors.

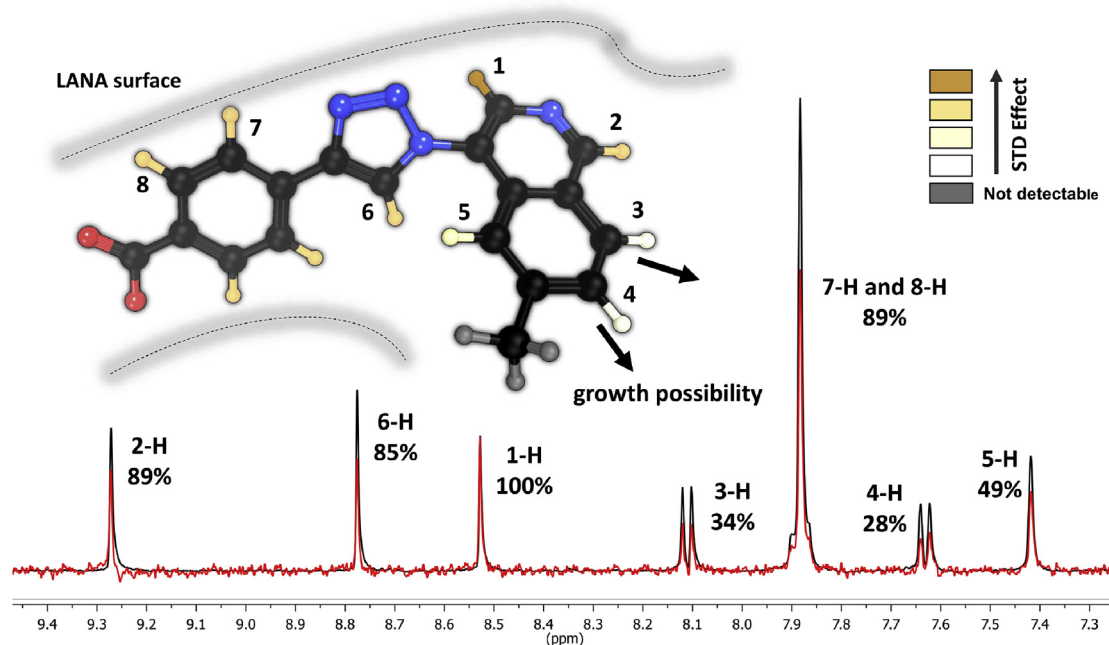
#### 3.4. STD-NMR studies for insight on ligand binding modes

Finally, we complemented our lead generation campaign by STD-NMR experiments with the aim to gather information on the binding orientation and to identify further growth vectors. In parallel, we attempted to solve co-crystal structures of our inhibitors in complex with LANA, unfortunately without success. However, we could successfully confirm previous STD-NMR and molecular docking results for inhibitor **I** by the obtained SAR in the present study and we were able to enlarge inhibitor **I** in the suggested direction. In order to inform our next optimization steps, we again performed STD-NMR experiments of our best inhibitor **50a**.

The protons of the tested compound, which are in closest proximity to the protein surface upon binding, are showing the



**Fig. 4.** Illustration of the nine single point mutations (yellow) of oligomerization interface and basic patch LANA mutant (blue) bound to DNA (red) assuming that our inhibitors bind at the LANA-DNA interaction interface. (For interpretation of the references to colour in this figure legend, the reader is referred to the Web version of this article.)



**Fig. 5.** STD experiments of compound **50a** in complex with LANA DBD mutant. The reference spectrum is displayed in black (STD-off) and STD difference spectra (STD-on) in red. Overlaid spectra were normalized to the signal for 1-H, which showed the strongest enhancement. (For interpretation of the references to colour in this figure legend, the reader is referred to the Web version of this article.)

strongest STD effects. In Fig. 5 an overlay of the on- (red) and off- (black) resonance STD-NMR spectra of the aromatic region are shown. The spectra were normalized to the strongest signal, which was observed for proton 1. The STD effects were calculated for each proton of inhibitor **50a** ( $\text{Effect}_{\text{STD}} = I/I_0$ ). The results suggest that compound **50a** has a binding orientation to LANA similar to that of inhibitor **I** [11].

The nitrogen of the pyridine ring presumably acts as a proton acceptor and thereby anchors proton 1 close to the LANA surface. The proton in position 2 showed also a strong STD effect of 89%. The corresponding proton in inhibitor **I** showed a slightly stronger effect of 100% [11]. The bulky isoquinoline moiety and the additional methyl group cause an *ortho* effect, which hinders the rotation of the bond between the triazole core and the isoquinoline. We

hypothesize, that this effect brings the nitrogen in an even more favorable orientation to the LANA surface and in turn leaves proton 2 now slightly more exposed. Furthermore, proton 6 located in the triazole core shows a stronger STD effect of 85% (47% in inhibitor **I**) [11], which leads us to suspect that the triazole is also now interacting more favourably with LANA. The four protons at the benzoic acid moiety, 7-H and 8-H, were found under one signal displaying a prominent STD effect of 89%. In contrast, the protons at the second ring of the isoquinoline motif showed a significantly lower STD effect (3-H: 34%, 4-H: 28% and 5-H: 49%). Hence, we conclude that these protons are not in direct contact with the protein and should be further investigated as potential secondary growth vectors. Unfortunately, the STD effect of the methyl group could not be determined, because signals of buffer ingredients were in the same

chemical shift range. For future medicinal chemistry optimization studies, further growing of the isoquinoline analogues in positions 3, 4 and 5 should be investigated. Additionally, a combination of the isoquinoline **50a** and compounds elongated in position 2 (see **19n** and **26a**) should be attempted.

#### 4. Conclusion

In this study we synthesized a series of new derivatives of our LANA inhibitor **I** [11] and evaluated them for LANA-DNA interaction inhibition in an FP-assay and in EMSA experiments in order to generate more potent LANA-DNA inhibitors. Based on the previously discovered fragment-sized inhibitor **I**, medicinal chemistry optimization lead to new inhibitors with improved potency. In particular, the replacement of the pyridine core (inhibitor **I**) by a methyl-isoquinoline (**50a**) led to an increase of inhibitory potency of 7-fold against the wild-type LANA CTD interaction with viral LBS1. Moreover, compound **50a** was also able to inhibit the interaction between LANA DBD mutant and LBS1+2 and LBS2+1 + 3, respectively, in the lower micromolar range. Additionally, step-by-step modification studies gave new and important SAR insights for future medicinal chemistry optimizations towards lead structures. Furthermore, STD-NMR measurements of the most potent inhibitor **50a** in complex with LANA revealed important details about the binding orientation and allowed for the identification of a new potential growth vector. The ability to inhibit the wild-type LANA DNA interaction in a low micro molar range ( $IC_{50}$   $60 \pm 4 \mu\text{M}$ ) with such a small molecule scaffold is striking as such a macromolecule-macromolecule-interaction is usually considered to be highly challenging, if not “undruggable”. Unexpectedly, we were able to significantly improve the inhibitory effects of our inhibitors using a chemistry-driven approach without having any structural information from a co-crystal about the binding mode and location on the LANA surface. Our results pave the way for the generation of a LANA-targeting anti-KSHV agent.

#### 5. Experimental section

All reagent-grade chemicals were purchased from commercial suppliers and were used as received. The purifications were performed using automated column flash chromatography (Combi-Flash Rf+, Teledyne ISCO, Lincoln, NE, USA) on silica gel 0.04–0.063 mm (RediSep Rf Kartuschen, Axel Semrau, Spocklhövel, Germany) or using preparative high performance liquid chromatography (HPLC, Ultimate 3000 UHPLC + focused, Thermo Scientific) on a reversed-phase column (C18 column, 5  $\mu\text{m}$ , Macherey-Nagel, Germany). The solvents used for column flash chromatography were EtOAc and cyclohexane or DCM and MeOH. The solvents used for HPLC were water (containing 0.05% [v/v] FA) and MeCN (containing 0.05% [v/v] FA) (gradient elution, MeCN:H<sub>2</sub>O 1:9  $\rightarrow$  9:1). Reaction progress was monitored by TLC on TLC Silica Gel 60 F<sub>254</sub> plates (Merk, Darmstadt, Germany) or by a reversed-phase liquid chromatography mass spectrometer (LCMS). <sup>1</sup>H and <sup>13</sup>C NMR were recorded on a Bruker Fourier spectrometers (500 or 126 MHz). Chemical shifts ( $\delta$ ) were reported in parts per million (ppm) relative to the corresponding reference solvent. The chemical shifts recorded as  $\delta$  values in ppm units by reference to the hydrogenated residues of the deuterated solvent as the internal standard. Coupling constants (*J*) are given in hertz (Hz) and splitting patterns are designated as follows: s, singlet; d, doublet; dd, doublet of doublets; t, triplet; m, multiplet; br., broad signal. Purity of all final compounds was measured on the UV trace recorded at a wavelength of 254 nm and was determined to be >95% by a reversed-phase liquid chromatography mass spectrometer (LCMS). Representative <sup>1</sup>H and <sup>13</sup>C spectra of all final compounds can be

found in the supporting information. High resolution mass spectra of all final compounds were measured on a Thermo Scientific Q Exactive Focus (Germany) equipped with a DIONEX ultimate 3000 UHPLC + focused and can be found in the supporting information. The reactions and purification steps were not optimized regarding yields.

**General procedure for azide formation (GP1) for Compounds 2, 18a-n, 21, 25a-b, 30a-b, 33a-b, 39a-e, 42, 45, 49a-c:** The appropriate aryl amine (1 eq.) was dissolved in EtOAc, cooled to 0 °C and 6 M HCl was added. Sodium nitrite (1.7 eq.) was dissolved in water and added slowly. The reaction mixture was stirred for 30 min at 0 °C. Subsequently, sodium azide (1.7 eq.) in water was added slowly at 0 °C. The mixture was stirred at room temperature for 2 h. TLC control indicated full conversion and the mixture was basified with saturated NaHCO<sub>3</sub> solution and was extracted with EtOAc (2  $\times$ ). The combined organic layers were dried over sodium sulfate and concentrated under reduced pressure to give the crude. The crude product was used as obtained in the next step without further purifications. Compound **2** is presented as an example. 3-azidopyridine (**2**): The azide was synthesized according to **GP1** using pyridin-3-amine **1** (376 mg, 4 mmol), sodium nitrite (1.7 eq., 469 mg, 6.8 mmol), sodium azide (1.7 eq., 442 mg, 6.8 mmol), EtOAc (8 mL), 6 M HCl (5 mL). The crude product (245 mg, 2 mmol, 50%) was used as obtained in the next step without further purifications.  $R_f = 0.37$  (PE/EtOAc 7:3).

**General procedure for synthesis of amino isoquinolin derivatives (GP2) for compounds 48a-c:** Under argon atmosphere the appropriate bromo isoquinolin (1 eq.), L-proline (0.1 eq.), sodium azide (1.3 eq.) and sodium carbonate (1.3 eq.) was dissolved in a 2:1 mixture of DMF and water. Subsequently, sodium ascorbate (1.3 eq.) and copper sulfate hepta hydrate (1 eq.) were added and the reaction mixture was stirred over night at 85 °C. After full conversion (LCMS control) the mixture was cooled to room temperature and EtOAc and sat. aqueous NaHCO<sub>3</sub> solution were added. The mixture was extracted with EtOAc (3x), the combined organic layers were dried over sodium sulfate and concentrated under reduced pressure to obtain the crude. The obtained products were used as obtained without further purification. Compound **48a** is presented as an example. 6-methylisoquinolin-4-amine (**48a**): The amino isoquinolin was synthesized according to **GP2** using 4-bromo-6-methylisoquinoline **47a** (100 mg, 0.46 mmol), L-proline (0.1 eq., 0.05 mmol, 5 mg), sodium azide (1.3 eq., 0.60 mmol, 34 mg), sodium carbonate (1.3 eq., 0.60 mmol, 64 mg), sodium ascorbate (1.3 eq., 0.60 mmol, 119 mg), copper sulfate heptahydrate (1 eq., 0.46 mmol, 115 mg), DMF (4 mL) and water (2 mL). The crude product (70 mg, 0.44 mmol, 97%) was used as obtained in the next step without further purifications. MS (ESI+) *m/z* 159 (M + H).

**General procedure for copper catalyzed click reaction (GP3) for compounds 3–11, 13, 16, 19a-n, 22, 26a-b, 31a-b, 34a-b, 40a-e, 50a-c:** Under argon atmosphere the appropriate alkyne (1 eq.) was suspended in a 1:1 mixture of water and MeOH. Subsequently, DIPEA (2.0 eq.), copper sulfate hepta hydrate (0.5 eq.) and sodium ascorbate (0.5 eq.) were added. After addition of the corresponding azide (1.2 eq.) the mixture was stirred for 16 h at room temperature. After full conversion (LCMS control) the mixture was acidified with 1 M HCl and the product was precipitated. The solids were collected, washed with water, and dried under vacuum to obtain the crude product. The products were purified using preparative HPLC. The solvents used were water (containing 0.05% [v/v] FA) and MeCN (containing 0.05% [v/v] FA) (gradient elution, MeCN:H<sub>2</sub>O 1:9  $\rightarrow$  9:1). Compound **4** is presented as an example. 3-(1-(pyridin-3-yl)-1H-1,2,3-triazol-4-yl)benzoic acid (**4**): The triazole was synthesized according to **GP3** using 3-ethynylbenzoic acid (92 mg, 0.64 mmol) and 3-azidopyridine **2** (1.3 eq., 100 mg, 0.83 mmol) as starting materials. The crude was obtained as a white solid (110 mg,

0.41 mmol, 64%). Purification was done using preparative HPLC.  $^1\text{H}$  NMR (500 MHz, DMSO- $d_6$ )  $\delta$  ppm 7.66 (br. s., 1 H) 7.68–7.79 (m, 1 H) 7.88–8.06 (m, 1 H) 8.19 (d,  $J = 7.63$  Hz, 1 H) 8.41 (d,  $J = 8.24$  Hz, 1 H) 8.53 (s., 1 H) 8.76 (s., 1 H) 9.25 (s., 1 H) 9.55 (s, 1 H) 13.23 (br. s., 1 H);  $^{13}\text{C}$  NMR (126 MHz, DMSO- $d_6$ )  $\delta$  ppm 120.56, 124.96, 127.82, 129.40, 141.24, 146.80, 149.81, 167.30.

**General procedure for Suzuki coupling (GP4) for compounds 24a-b, 29a-b, 35a-l:** Under argon atmosphere the appropriate aryl halide 1 (eq.) was dissolved in water and 1,4-dioxane (1:1). Sodium carbonate (3 eq.), the corresponding boronic acid (1.2 eq.) and tetrakis (triphenylphosphine) palladium (0.1 eq.) were added. The reaction mixture was heated to 90 °C for 16 h. After full conversion (LCMS control) the mixture was cooled to room temperature and EtOAc and sat. aqueous  $\text{NaHCO}_3$  solution were added. The mixture was extracted with EtOAc (3x), the combined organic layers were dried over sodium sulfate and concentrated under reduced pressure to obtain the crude. The purification was done using automated flash chromatography (cyclohexane/EtOAc 1:0  $\rightarrow$  0:1). Compound **24a** is presented as an example. 2-(5-amino-4-methylpyridin-2-yl)phenol (**24a**): The coupling was done according to **GP4** using 6-bromo-4-methylpyridin-3-amine **23** (130 mg, 0.69 mmol), (2-hydroxyphenyl)boronic acid (1.2 eq., 113 mg, 0.83 mmol), sodium carbonate (3 eq., 218 mg, 2.08 mmol) and tetrakis (triphenylphosphine) palladium (0.1 eq., 78 mg, 0.07 mmol) in 1,4-dioxane:water (1:1, 6 mL). **24b** was obtained as yellow solid (103 mg, 0.52 mmol, 75%). MS (ESI+)  $m/z$  201 (M + H).

**General procedure for hydrolysis of methyl ester (GP5) for compounds 36a-l:** The appropriate methyl ester was dissolved in MeOH and aqueous 0.5 M NaOH solution (1:1). The mixture was stirred at room temperature for 16 h. After full conversion (LCMS control) the mixture was acidified with 1 M HCl and the product was precipitated. The solids were collected, washed with water, and dried under vacuum to obtain the crude product. The products were purified using preparative HPLC. Compound **36a** is presented as an example. 4-(1-(5-phenylpyridin-3-yl)-1H-1,2,3-triazol-4-yl) benzoic acid (**36a**): The synthesis was done according to **GP5** using methyl 4-(1-(5-phenylpyridin-3-yl)-1H-1,2,3-triazol-4-yl)benzoate **35a** (20 mg, 0.06 mmol). The crude was obtained as a white solid (13 mg, 0.04 mmol, 66%). Purification was done using preparative HPLC.  $^1\text{H}$  NMR (500 MHz, DMSO- $d_6$ )  $\delta$  ppm 7.49–7.54 (m, 1 H) 7.56–7.61 (m, 2 H) 7.84–7.95 (m, 2 H) 8.02–8.16 (m, 4 H) 8.65 (t,  $J = 2.21$  Hz, 1 H) 9.07 (d,  $J = 1.98$  Hz, 1 H) 9.22 (d,  $J = 2.29$  Hz, 1 H) 9.64 (s, 1 H);  $^{13}\text{C}$  NMR (126 MHz, DMSO- $d_6$ )  $\delta$  ppm 121.41, 125.29, 125.57, 127.30, 128.97, 129.30, 130.22, 133.38, 133.97, 135.68, 136.49, 139.93, 146.65, 147.70, 167.01.

**General procedure for Ullmann reaction (GP6) for compounds 38a-e:** Under argon atmosphere 6-bromo-4-methylpyridin-3-amine (1 eq.) was dissolved in DMF and the appropriate phenol derivative (1.2 eq.), cesium carbonate (3 eq.) and CuI (0.05 eq.) were added. The mixture was stirred for 16 h at 130 °C. LCMS control indicated full conversion and the mixture was cooled to room temperature. EtOAc and sat. aqueous  $\text{NaHCO}_3$  solution were added. The mixture was extracted with EtOAc (3x), the combined organic layers were dried over sodium sulfate and concentrated under reduced pressure to obtain the crude. Compound **38a** is presented as an example. 4-methyl-6-phenoxy pyridin-3-amine (**38a**): The aryl ether was synthesized according to **GP6** using 6-bromo-4-methylpyridin-3-amine **37** (100 mg, 0.53 mmol), phenol (1.2 eq., 0.60 mmol, 70 mg), cesium carbonate (3 eq., 1.61 mmol, 523 mg) and CuI (0.1 eq., 0.05 mmol, 9 mg) in DMF (3 mL). The product was purified using automated flash chromatography (DCM/MeOH 1:0  $\rightarrow$  9:1). Yield: (30 mg, 0.15 mmol, 28%) MS (ESI+)  $m/z$  201 (M + H).

**Protein expression and purification:** The expression and purification of His-tagged oligomerization-deficient LANA DNA

binding domain (DBD; aa1008–1146) mutant and GST-tagged KSHV LANA C-terminal domain (CTD; aa934–1162) were described previously and the protocol was adopted [10,11].

**Fluorescence Polarization (FP) assay:** The FP assay was performed, analyzed and evaluated as described previously [11].

**Electrophoretic mobility shift assay (EMSA):** The EMSA was performed, analyzed and evaluated as described previously [11].

**Saturation-Transfer Difference (STD) NMR:** The STD experiments were recorded at 298 K on a Bruker Fourier spectrometer (500 MHz). The samples contained 10  $\mu\text{M}$  (final concentration) His-tagged oligomerization-deficient LANA DBD (aa1008–1146) mutant and a final compound concentration of 500  $\mu\text{M}$ . The control spectra were recorded under the same conditions containing the free compound to test for artifacts. The STD buffer for experiments consists of 10 mM HEPES, 150 mM NaCl, pH 7.4 in  $\text{D}_2\text{O}$  containing 10% [v/v] DMSO- $d_6$ . The experiments were recorded with a carrier set at  $-1$  ppm for the on-resonance and  $-40$  ppm for the off-resonance irradiation. Selective protein saturation was carried out at 2 s by using a train of 50 ms Gauss-shaped pulses, each separated by a 1 ms delay.

## Declaration of competing interest

The authors declare that they have no known competing financial interests or personal relationships that could have appeared to influence the work reported in this paper.

## Acknowledgments

The authors acknowledge the financial support by the German Centre for Infection Research (DZIF) and the DFG Collaborative Research Centre 900, project C1.

## Appendix A. Supplementary data

Supplementary data to this article can be found online at <https://doi.org/10.1016/j.ejmech.2020.112525>.

## References

- [1] M. Weidner-Glunde, G. Mariggio, T.F. Schulz, Kaposi's sarcoma-associated herpesvirus latency-associated nuclear antigen: replicating and shielding viral DNA during viral persistence, *J. Virol.* 91 (2017), <https://doi.org/10.1128/JVI.01083-16>.
- [2] L. Wang, B. Damania, Kaposi's sarcoma-associated herpesvirus confers a survival advantage to endothelial cells, *Canc. Res.* 68 (2008) 4640–4648, <https://doi.org/10.1158/0008-5472.CAN-07-5988>.
- [3] P. Purushothaman, P. Dabral, N. Gupta, R. Sarkar, S.C. Verma, KSHV genome replication and maintenance, *Front. Microbiol.* 7 (2016) 54, <https://doi.org/10.3389/fmicb.2016.00054>.
- [4] G. Mariggio, S. Koch, G. Zhang, M. Weidner-Glunde, J. Rückert, S. Kati, S. Santag, T.F. Schulz, Kaposi Sarcoma Herpesvirus (KSHV) Latency-Associated Nuclear Antigen (LANA) recruits components of the MRN (Mre11-Rad50-NBS1) repair complex to modulate an innate immune signaling pathway and viral latency, *PLoS Pathog.* 13 (2017), e1006335, <https://doi.org/10.1371/journal.ppat.1006335>.
- [5] D.H. Kedes, E. Operskalski, M. Busch, R. Kohn, J. Flood, D. Ganem, The seroepidemiology of human herpesvirus 8 (Kaposi's sarcoma-associated herpesvirus): distribution of infection in KS risk groups and evidence for sexual transmission, *Nat. Med.* 2 (1996) 918–924, <https://doi.org/10.1038/nm0896-918>.
- [6] L. Yan, V. Majeriac, Z.-M. Zheng, K. Lan, Towards better understanding of KSHV life cycle: from transcription and posttranscriptional regulations to pathogenesis, *Virol. Sin.* 34 (2019) 135–161, <https://doi.org/10.1007/s12250-019-00114-3>.
- [7] L. Rainbow, G.M. Platt, G.R. Simpson, R. Sarid, S.J. Gao, H. Stoiber, C.S. Herrington, P.S. Moore, T.F. Schulz, The 222- to 234-kilodalton latent nuclear protein (LANA) of Kaposi's sarcoma-associated herpesvirus (human herpesvirus 8) is encoded by orf73 and is a component of the latency-associated nuclear antigen, *J. Virol.* 71 (1997) 5915–5921.
- [8] T. Uppal, S. Banerjee, Z. Sun, S.C. Verma, E.S. Robertson, KSHV LANA—the master regulator of KSHV latency, *Viruses* 6 (2014) 4961–4998, <https://doi.org/10.3390/v6114961>.

- [doi.org/10.3390/v6124961](https://doi.org/10.3390/v6124961).
- [9] F. Juillard, M. Tan, S. Li, K.M. Kaye, Kaposi's sarcoma herpesvirus genome persistence, *Front. Microbiol.* 7 (2016) 1149, <https://doi.org/10.3389/fmicb.2016.01149>.
- [10] J. Hellert, M. Weidner-Glunde, J. Krausze, U. Richter, H. Adler, R. Fedorov, M. Pietrek, J. Rückert, C. Ritter, T.F. Schulz, et al., A structural basis for BRD2/4-mediated host chromatin interaction and oligomer assembly of Kaposi sarcoma-associated herpesvirus and murine gammaherpesvirus LANA proteins, *PLoS Pathog.* 9 (2013), e1003640, <https://doi.org/10.1371/journal.ppat.1003640>.
- [11] P. Kirsch, V. Jakob, K. Oberhausen, S.C. Stein, I. Cucarro, T.F. Schulz, M. Empting, Fragment-based discovery of a qualified hit targeting the latency-associated nuclear antigen of the oncogenic kaposi's sarcoma-associated herpesvirus/human herpesvirus 8, *J. Med. Chem.* 62 (2019) 3924–3939, <https://doi.org/10.1021/acs.jmedchem.8b01827>.
- [12] K.R. Alkharsah, T.F. Schulz, A role for the internal repeat of the Kaposi's sarcoma-associated herpesvirus latent nuclear antigen in the persistence of an episomal viral genome, *J. Virol.* 86 (2012) 1883–1887, <https://doi.org/10.1128/JVI.06029-11>.
- [13] A. de Leo, Z. Deng, O. Vladimirova, H.-S. Chen, J. Dheekollu, A. Calderon, K.A. Myers, J. Hayden, F. Keeney, B.B. Kaufer, et al., LANA oligomeric architecture is essential for KSHV nuclear body formation and viral genome maintenance during latency, *PLoS Pathog.* 15 (2019), e1007489, <https://doi.org/10.1371/journal.ppat.1007489>.
- [14] R.K. Singh, Z.L. Lamplugh, F. Lang, Y. Yuan, P. Lieberman, J. You, E.S. Robertson, KSHV-encoded LANA protects the cellular replication machinery from hypoxia induced degradation, *PLoS Pathog.* 15 (2019), e1008025, <https://doi.org/10.1371/journal.ppat.1008025>.
- [15] S.C. Verma, K. Lan, E. Robertson, Structure and function of latency-associated nuclear antigen, *Curr. Top. Microbiol. Immunol.* 312 (2007) 101–136.
- [16] F. Wei, J. Gan, C. Wang, C. Zhu, Q. Cai, Cell cycle regulatory functions of the KSHV oncoprotein LANA, *Front. Microbiol.* 7 (2016) 334, <https://doi.org/10.3389/fmicb.2016.00334>.
- [17] J. Hellert, M. Weidner-Glunde, J. Krausze, H. Lünsdorf, C. Ritter, T.F. Schulz, T. Lührs, The 3D structure of Kaposi sarcoma herpesvirus LANA C-terminal domain bound to DNA, *Proc. Natl. Acad. Sci. U.S.A.* 112 (2015) 6694–6699, <https://doi.org/10.1073/pnas.1421804112>.
- [18] C. Parravicini, B. Chandran, M. Corbellino, E. Berti, M. Paulli, P.S. Moore, Y. Chang, Differential viral protein expression in Kaposi's sarcoma-associated herpesvirus-infected diseases : Kaposi's sarcoma, primary effusion lymphoma, and multicentric Castlemans disease, *Am. J. Pathol.* 156 (2000) 743–749.
- [19] N. Coen, S. Duraffour, R. Snoeck, G. Andrei, KSHV targeted therapy: an update on inhibitors of viral lytic replication, *Viruses* 6 (2014) 4731–4759, <https://doi.org/10.3390/v6114731>.
- [20] C. Hoffmann, M. Sabranski, S. Esser, HIV-associated kaposi's sarcoma, *Oncol. Res. Treat.* 40 (2017) 94–98, <https://doi.org/10.1159/000455971>.
- [21] P. Kirsch, V. Jakob, W.A.M. Elgaher, C. Walt, K. Oberhausen, T.F. Schulz, M. Empting, Discovery of novel latency-associated nuclear antigen inhibitors as antiviral agents against kaposi's sarcoma-associated herpesvirus, *ACS Chem. Biol.* (2020), <https://doi.org/10.1021/acscchembio.9b00845>.
- [22] J. Cui, L.A. Hu, W. Shi, G. Cui, X. Zhang, Q.-W. Zhang, Design, synthesis and anti-platelet aggregation activity study of ginkgolide-1,2,3-triazole derivatives, *Molecules* 24 (2019), <https://doi.org/10.3390/molecules24112156>.
- [23] D. Dou, G. He, Y. Li, Z. Lai, L. Wei, K.R. Alliston, G.H. Lushington, D.M. Eichhorn, W.C. Groutas, Utilization of the 1,2,3,5-thiatriazolidin-3-one 1,1-dioxide scaffold in the design of potential inhibitors of human neutrophil proteinase 3, *Bioorg. Med. Chem.* 18 (2010) 1093–1102, <https://doi.org/10.1016/j.bmc.2009.12.057>.
- [24] Y. Liu, Q. Xiao, Y. Liu, Z. Li, Y. Qiu, G.-B. Zhou, Z.-J. Yao, S. Jiang, Biological evaluation of new mimetics of annonaceous acetogenins: alteration of right scaffold by click linkage with aromatic functionalities, *Eur. J. Med. Chem.* 78 (2014) 248–258, <https://doi.org/10.1016/j.ejmech.2014.03.062>.
- [25] J. Hellert, J. Krausze, T.F. Schulz, T. Lührs, Crystallization, room-temperature X-ray diffraction and preliminary analysis of Kaposi's sarcoma herpesvirus LANA bound to DNA, *Acta Crystallogr. F Struct. Biol. Commun.* 70 (2014) 1570–1574, <https://doi.org/10.1107/S2053230X14019906>.